Tracking and understanding the first-order structural transition in Er_5Si_4

Y. Mozharivskyj,[1] A. O. Pecharsky,[1] V. K. Pecharsky,[1,2] G. J. Miller,[3,*] and K. A. Gschneidner, Jr.[1,2]
[1]*Ames Laboratory, Iowa State University, Ames, Iowa 50011-3020, USA*
[2]*Department of Materials Science and Engineering, Iowa State University, Ames, Iowa 50011-2300, USA*
[3]*Department of Chemistry, Iowa State University, Ames, Iowa 50011-3110, USA*
(Received 7 October 2003; revised manuscript received 24 November 2003; published 1 April 2004)

Temperature-dependent single crystal x-ray-diffraction studies revealed a reversible first-order phase transition in Er_5Si_4. The high-temperature phase adopts the orthorhombic Gd_5Si_4-type structure, and the low-temperature phase has the monoclinic $Gd_5Si_2Ge_2$-type structure. Unlike the magnetic/martensitic transition in $Gd_5Si_2Ge_2$, the structural change in Er_5Si_4 is not coupled with a magnetic transition, and the structural sequence below room temperature is just the reverse. A vibrational mode that breaks half of the interslab silicon dimers and rotates slabs in the monoclinic structure, thus lowering the symmetry from $Pnma$ to $P112_1/a$, has been identified using Landau theory. While the monoclinic phase is electronically stabilized at low temperatures, the orthorhombic phase is entropically preferable at high temperatures.

DOI: 10.1103/PhysRevB.69.144102 PACS number(s): 61.10.−i, 61.50.Ks, 71.20.−b

INTRODUCTION

The 1967 studies of R_5Si_4 and R_5Ge_4 phases (R=Gd, Tb, Dy, Ho, and Er)[1] were followed by the discovery of the giant magnetocaloric effect in $Gd_5Si_2Ge_2$ thirty years later.[2–4] A magnetic/martensitic transition that occurs in $Gd_5Si_2Ge_2$ around 300 K makes it a promising candidate for near room temperature magnetic refrigeration.[5,6] Attempts to understand this unusual phenomenon and a quest for new materials exhibiting similar properties have led to a broad research effort targeting $R_5Si_{4-x}Ge_x$ and related compounds.[7–16] A considerable body of knowledge, accumulated during the last seven years, enables a much better understanding of the central problem pertaining to $Gd_5Si_2Ge_2$ and related phases, namely, an intimate relationship between chemical composition and crystal structure, and a strong dependence of the latter on temperature, magnetic field, and pressure.[7,8,17] Ferromagnetic ordering in $Gd_5Si_2Ge_2$ is coupled with structural changes: the low-temperature ferromagnetic polymorph adopts an orthorhombic Gd_5Si_4-type structure with T-T dimers between slabs (T represents Si and Ge atoms mixed together in the corresponding lattice sites); the high-temperature paramagnetic form has a monoclinic $Gd_5Si_2Ge_2$-type structure, in which half of the T-T interslab dimers are broken.[18] The T-T bond cleavage and associated slab movement by $\sim$0.2 Å can be controlled through the Ge/Si ratio, magnetic field, temperature, and pressure.[7,17,19]

Among many of the unusual features of the magnetic/martensitic phase transition in $Gd_5Si_2Ge_2$ is the fact that the low-temperature structure has a higher symmetry ($Pnma$) than the high-temperature structure ($P112_1/a$), although temperature dependence of the Gibbs free energy on entropy dictates the reverse structural sequence.[20] Calculations by Choe *et al.*[28] and later by Pecharsky *et al.*[21] have shown that this phase sequence arises from the large magnetic exchange coupling, which is optimized in the orthorhombic phase due to higher valence electron concentration available for metallic bonding. The magnetic exchange energy is sufficiently large to overcome the unfavorable entropy contribution even near room temperature. However, if monoclinic $Gd_5Si_2Ge_2$ is annealed between $\sim$500 and $\sim$750 K, it irreversibly transforms into the orthorhombic Gd_5Si_4-type phase.[21,22] From the Gibbs free energy/entropy relationship this is indeed the expected structural transition. Both theoretical predictions[21] and our ongoing studies indicate that the high-temperature monoclinic-to-orthorhombic transition may be triggered by changes in the Si/Ge site occupancies. In view of the present day knowledge, a system that allows full decoupling of the crystal structure from chemical composition and magnetic field effects, while preserving the structure-temperature relationships, is highly desirable for testing forthcoming theoretical models. Recent studies of the physical properties of Er_5Si_4 indicated a first-order phase transition around 200 to 230 K without any magnetic ordering.[23] In this work, we present crystallographic and electronic structure analyses of this transformation. We were able to observe temporally and spatially resolved transformation of the monoclinic and orthorhombic lattices, which provides multiple clues for understanding the mechanism of the transition at the atomic level.

X-RAY CRYSTALLOGRAPHIC STUDIES

A barlike crystal ($0.02\times0.02\times0.1$ mm^3) was extracted from the bulk $Er_{5.05}Si_4$ alloy prepared by arc melting of erbium and silicon. Room temperature x-ray-diffraction data (Mo $K\alpha$ radiation) were collected in a reciprocal hemisphere on a Bruker SMART Apex CCD diffractometer. Low-temperature data were collected at 173, 203, 208, 213, 222, 223, 228, 233, and 243 K in a reciprocal sphere on a Bruker SMART 1000 CCD diffractometer with Mo $K\alpha$ radiation; the temperature was stable to $\pm$1 K with respect to the value set for an experiment. The data were harvested by collecting three sets of 606 frames with 0.3° scans in ω with an exposure time of 10 s per frame. The range of 2θ extended from 4° to 57°. Integrated intensities were extracted and then corrected for Lorentz and polarization effects through the SAINT program.[24] For the twinned crystal, orientation matrices of the two twin components were used during the integration and intensities of the overlapping reflections of the two components were not separated. The unit cell dimensions were

TABLE I. Crystal data and structure refinements of Er_5Si_4.

Temperature, K	203(1)	293(1)
Space group	$P112_1/a$[a]	$Pnma$
Lattice parameters, Å	$a=7.3460(9)$	$a=7.2838(6)$
	$b=14.3752(18)$	$b=14.3627(11)$
	$c=7.5571(9)$, $\gamma=92.992(2)°$	$c=7.5943(6)$
Z	4	4
Density (calculated), g/cm^3	7.907	7.931
Index ranges	$-9\leqslant h\leqslant 9$, $-19\leqslant k\leqslant 19$, $-9\leqslant l\leqslant 9$	$-9\leqslant h\leqslant 9$, $-18\leqslant k\leqslant 17$, $-9\leqslant l\leqslant 10$
Independent reflections	3610[b]	989
Completeness to $2\theta=57°$	96.2%	97.1%
Data/parameters	3610/84	989/47
Goodness-of-fit on F^2	1.003	1.195
Final R indices $[I/\sigma(I)>2]$	$R_1=0.0434$, $wR_2=0.0709$	$R_1=0.0259$, $wR_2=0.0572$
R indices (all data)	$R_1=0.0753$, $wR_2=0.0761$	$R_1=0.0284$, $wR_2=0.0582$
Extinction coefficient	0.00057(2)	0.00067(7)
Largest diff. peak/hole, e./Å^3	3.245/−2.935	2.076/−2.165

[a]Standard setting for the monoclinic structure is $P12_1/c1$ with $a=14.3752(18)$, $b=7.5571(9)$, $c=7.3460(9)$ Å, $\beta=92.992(2)°$ and can be achieved through the following cyclic permutation of the unit cell vectors **a**, **b**, **c**→**b**, **c**, **a**. The above setting ($P112_1/a$) is used so that a direct comparison can be made with the orthorhombic structure.

[b]Symmetry equivalent reflections are treated as independent during the twin refinement.

refined using all observed Bragg reflections after integration.

The empirical absorption correction for the untwinned crystal (above 222 K) was based on modeling a transmission surface by spherical harmonics employing equivalent reflections with $I/\sigma(I)>3$ (program SADABS[24]); for the twinned crystal (below 222K) it was done by modeling a transmission surface of each twinned component by spherical harmonics using overlapping and nonoverlapping equivalent reflections with $I/\sigma(I)>3$ (program TWINABS[24]). The structure solutions were obtained by direct methods and refined on F^2 by the full-matrix, least-squares method (program SHELXL[24]). The atomic parameters for the monoclinic polymorph at 173, 203, 208, and 213 K and for the orthorhombic structure at 223, 228, 233, 243, and 293 K are within three standard deviations from one another for the same symmetry. The structural data for the monoclinic crystal at 203 K and for the orthorhombic crystal at 293 K are listed in Tables I and II.

Since the crystal was extracted from the off-stoichiometric $Er_{5.05}Si_4$ alloy, potential deficiencies on the Si sites were verified. Relaxing the Si occupancies during the final refinement cycles for the room temperature data did not lead to lower R values and the occupancy factors were within two standard deviations from unity: 1.00(1) for Si1, 0.97(2) for Si2, and 0.97(2) for Si3. Two more crystals were randomly extracted from the same $Er_{5.05}Si_4$ alloy and their x-ray diffraction data were collected at room temperature. The refinements yielded no statistically significant deviations of the occupancy factors from unity, thus indicating that the crystal compositions can be represented as Er_5Si_4. Defects on Si sites, if any, are too small to be detected using x-ray diffraction technique due to unknown displacement parameters of the Si atoms. It is worth noting that the third crystal produced additional diffraction spots that were indexed as hexagonal Er_5Si_3 (program GEMINI[24]), which is expected from the phase diagram of the Er-Si system[25] assuming a fully stoichiometric Er_5Si_4 phase.

EXPERIMENTAL RESULTS AND DISCUSSION

Monoclinic twin law and components at 203 K and below

Bragg reflections observed at 203(1) K, could not be indexed in the orthorhombic lattice observed at room tempera-

TABLE II. Atomic and equivalent isotropic displacement parameters (U_{eq}, Å^2) for Er_5Si_4. (Anisotropic temperature factors and other crystallographic details can be obtained from the authors upon request.)

Atom	x/a	y/b	z/c	U_{eq}
		203 K		
Er1A	−0.00355(7)	0.59762(4)	0.18031(8)	0.0043(1)
Er1B	0.01782(7)	0.90166(4)	0.18089(8)	0.0042(1)
Er2A	0.32896(7)	0.12239(4)	0.17835(8)	0.0033(1)
Er2B	0.35346(7)	0.37920(4)	0.16654(8)	0.0039(1)
Er3	0.17404(9)	0.25341(4)	0.50624(7)	0.0035(1)
Si1A	0.1515(5)	0.0399(3)	0.4713(5)	0.0039(8)
Si1B	0.2002(5)	0.4584(3)	0.4635(5)	0.0053(9)
Si2	0.0457(4)	0.2489(3)	0.1087(4)	0.0038(8)
Si3	0.2910(5)	0.2481(3)	0.8684(4)	0.0048(8)
		293 K		
Er1	0.01987(5)	0.59614(3)	0.18016(4)	0.0084(1)
Er2	0.32293(5)	0.12320(3)	0.17864(4)	0.0072(1)
Er3	0.15473(6)	1/4	0.51179(6)	0.0072(2)
Si1	0.1540(3)	0.0391(2)	0.4703(3)	0.0093(6)
Si2	0.0262(4)	1/4	0.1048(4)	0.0093(6)
Si3	0.2737(4)	1/4	0.8704(4)	0.0085(6)

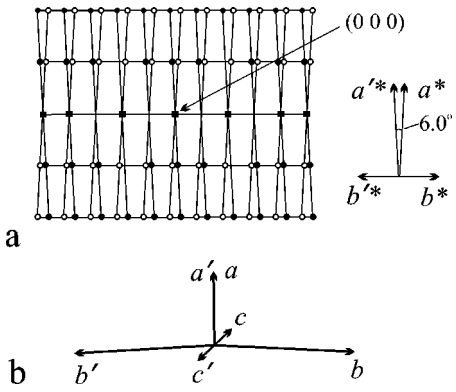

FIG. 1. (a) Projections of reflections with $I>2\sigma(I)$, $-2\leqslant h\leqslant 2$, $-5\leqslant k\leqslant 5$, $-9\leqslant l\leqslant 9$ on the a^*b^* plane in the reciprocal space. The open circles represent the reflections from the dominant monoclinic twin component, the solid circles show the reflections from the secondary twin component and solid squares represent the fully overlapped reflections that belong to both components. (b) Monoclinic twin law in Er_5Si_4 below 222 K. The a axis is the twin axis.

ture. Analysis of the reflections with $I\geqslant 2\sigma(I)$ indicated that they can be assigned to two monoclinic lattices with $a^*\approx 1/7.35$ Å, $b^*\approx 1/14.37$ Å, $c^*\approx 1/7.56$ Å, and $\gamma^*\approx 87°$ (Fig. 1). The two lattices are superimposed in the b^*c^* plane and they can be mutually transformed through 180° rotation around the normal to the b^*c^* plane, i.e., by 180° rotation around the a axis in real space [similar twinning was observed in $Gd_5Si_2Ge_2$ (Refs. 18, 26)]. The two reciprocal lattices coincide when h and $h'=5n$, $n=0$, 1, 2 [see Fig. 1(a)]. Overlapped reflections with $h=h'=5n$ do not differ in shape from nonoverlapped reflections with h and $h'\neq 5n$, indicating a nearly perfect superposition of the two lattices at these reciprocal points. The remaining reflections are well separated, indicating a pseudomerohedral[27] rotational twin with respect to the a axis (rotation by 180° around the [100] crystallographic direction). As illustrated in Fig. 1(b), the twin law, i.e., a matrix transforming the axes of one twin component into those of the other, is

$$\mathbf{a}'=\mathbf{a},$$

$$\mathbf{b}'=-\mathbf{b}+2\mathbf{a}\left(\frac{b}{a}\right)\cos\gamma$$

$$=-\mathbf{b}-0.2046\mathbf{a}$$

$$\approx-\mathbf{b}-\frac{1}{5}\mathbf{a},$$

$$\mathbf{c}'=-\mathbf{c},$$

$$\begin{pmatrix}\mathbf{a}'\\ \mathbf{b}'\\ \mathbf{c}'\end{pmatrix}=\begin{pmatrix}1 & 0 & 0\\ -\frac{1}{5} & -1 & 0\\ 0 & 0 & -1\end{pmatrix}\begin{pmatrix}\mathbf{a}\\ \mathbf{b}\\ \mathbf{c}\end{pmatrix}.$$

The same matrix describes the $hkl\rightarrow h'k'l'$ transformation in reciprocal space,[28,29] and because of this twin law, the two reciprocal lattices coincide almost exactly at $h=5n$ ($k'=-1/5h-k$).

The volume ratio between the two twin components of the same crystal was refined at the same temperature during three independent cooling cycles and at three different temperatures during the first heating. The twin ratio remains constant within three standard deviations after the orthorhombic to monoclinic transition took place, e.g., during the first heating the fraction of the minor component was 0.260(1) at 173 K and 0.254(1) at 203 K. The twin ratio, however, changes upon cycling through the transition, e.g., the fraction of the minor component at 203 K was 0.254(1), 0.323(1), and 0.232(1) after the first, second, and third cooling, respectively. Despite considerable changes in phase volume, the repeated orthorhombic-to-monoclinic transition had no apparent damaging effect on the crystal: it remained intact after the third cycle. These two observations indicate that the twinning can originate at any point in the orthorhombic lattice, but once the monoclinic structure is formed, there is no transformation between the two monoclinic lattices. Another interesting feature is that the twin ratio was never close to 1:1, thus indicating that, at least for this particular specimen, twinning is not a stochastic process: there was always a dominant component and a minor component.

Formation of the orthorhombic lattice and disappearance of the monoclinic lattices

After the first cooling and during the subsequent heating, the temperature was increased by 1 K from 220 to 223 K and diffraction data were collected at each fixed temperature point. The orthorhombic Er_5Si_4 phase appeared 25 min after the temperature was raised from 221 to 222 K. It developed abruptly from the dominant monoclinic twin component, which is called component I thereafter, but not from the minor monoclinic twin component, which is called component II thereafter (Fig. 2). Although the orthorhombic lattice developed suddenly from the component I, further separation between the two lattices occurred for the next 8 min. While the monoclinic twin components have a common b^*c^* plane in reciprocal space, the orthorhombic lattice shares only the c^* axis with the monoclinic lattices [Fig. 3(a)]. The orthorhombic reciprocal lattice is rotated around c^* in the way that the angle between $a^*_{\text{mon\_I}}$ and a^*_{orth} is 1.3° [Fig. 3(a)], and the angle between $b^*_{\text{mon\_I}}$ and b^*_{orth} is 1.7°, which is due to the fact that $\gamma^*_{\text{mon}}=180-\gamma_{\text{mon}}\approx 87°$ and $\gamma^*_{\text{orth}}=90°$.

During the transformation, all observed reflections could be indexed to the two original monoclinic lattices and the orthorhombic lattice as seen from the inset in Fig. 3(a). The lattice parameters of the two coexistent phases were obtained by the least-squares method from reflections collected when the three lattices were well separated spatially, which occurred 2 to 8 h after the temperature was stable at 222 K. The results for the monoclinic phase include both twin components $a_{\text{mon}}=7.370(3)$, $b_{\text{mon}}=14.405(6)$, $c_{\text{mon}}=7.575(3)$ Å, $\gamma_{\text{mon}}=92.95(1)°$ and $a_{\text{orth}}=7.291(2)$, $b_{\text{orth}}=14.377(4)$, $c_{\text{orth}}=7.604(2)$ Å. From the mutual orientation of the reciprocal lattices, the twin laws in direct space were obtained [Fig. 3(b)]. The monoclinic components I and II are rotation twins around the a axis, and their axial transformations are described by the matrix discussed above. The

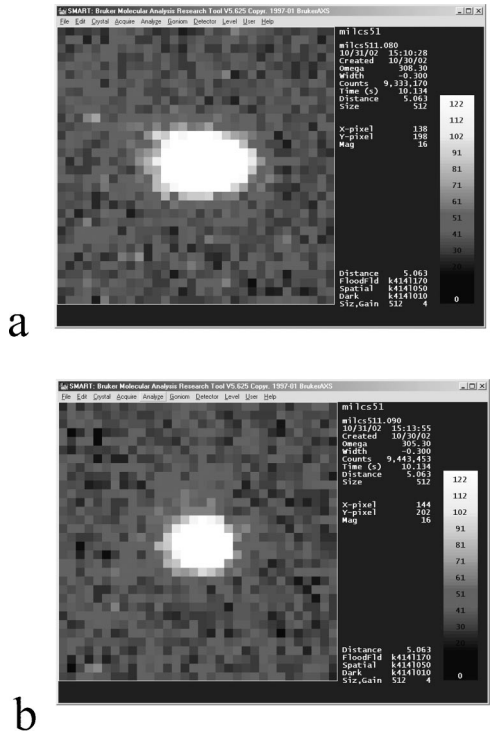

FIG. 2. Initial appearance of the orthorhombic phase at 222 K. The 2 −3 2 Bragg reflection from the monoclinic component I develops a shoulder (a) 25 min after temperature stabilization. The 2 −3 2 Bragg reflection corresponding to component II (b) shows no broadening. The reflections are 16 times magnified.

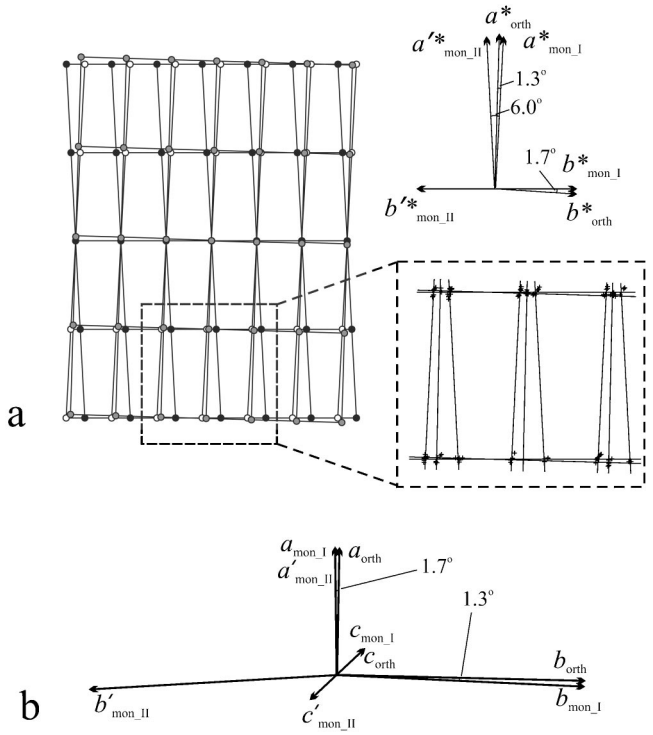

FIG. 3. (a) Mutual orientation of the reciprocal lattices of the dominant monoclinic twin component (open circles, component I), the minor monoclinic twin component (solid circles, component II) and the orthorhombic component (gray circles) of the Er_5Si_4 crystal at 222 K. The inset shows fitting the observed reflections, represented by crosses, with $I>2\sigma(I)$ and $-2\leqslant h\leqslant -1$, $-1\leqslant k\leqslant 1$, $-9\leqslant l\leqslant 9$ to the three lattices. (b) Schematic representation of the twin laws in real space. The twin axis between the two monoclinic components is the a_{mon} axis. The c axis is common for both monoclinic and orthorhombic phases.

orthorhombic lattice shares only the c axis with both monoclinic components, and since there is a discontinuous change in the lattice parameters (a feature intrinsic to any first-order transition), no matrix can be derived to account for the axial transformation between the monoclinic and orthorhombic lattices.

When a fraction of the orthorhombic component increased, a similar fraction of the monoclinic component I decreased, but the amount of the monoclinic component II did not change with time as long as two phases coexisted at 222 K. The fraction of each component was estimated by comparing intensities of strong nonoverlapping reflections (at least three reflections with h or $k\geqslant 3$) measured over four narrow time intervals. Indeed, this estimate is based on the assumption that the strong reflections in the orthorhombic phase are similar in intensity to the same ones in the monoclinic phase.[27,30–32] Right after the orthorhombic lattice was formed (about 30 min after the temperature increase, which is the reference point here) the ratio between the orthorhombic and monoclinic I components was 0.08(2), after 4.5 h it was 0.21(2), after 7.8 h 0.33(2), and after 9.5 h 0.30(2). During the last 2.5 h at 222(1) K no significant changes in the component ratio were detected.

9.5 h after the temperature was raised, the reflections of the monoclinic component II were observed closer to the reflections of the orthorhombic phase than they were earlier (Fig. 4). At the same time, the lattice of component I showed no noticeable distortion. Finally, the monoclinic phase transformed abruptly into the orthorhombic phase 10.3 h after the temperature was stabilized at 222 K. The transition was sudden since the two consecutive frames, 20 s apart in time, exhibited a different number of lattices. From that moment on, only reflections of the orthorhombic lattice were present in the diffraction pattern of this single crystalline specimen of Er_5Si_4. This time dependence of the completion of the phase transition at 222(1) K is quite unusual and may be related to larger that $\pm 1°$ temperature fluctuations. It is possible that the abrupt transformation after 10.3 h was caused by a short increase of the cooling gas temperature, or by a few degrees fluctuation in the temperature of the environment.

Phase transition

As illustrated in Fig. 5, both the magnetic susceptibility (measured on a Lake Shore magnetometer) and heat capacity (measured using a semi-adiabatic heat-pulse calorimeter) of Er_5Si_4 indicate a phase transition between ~205 and ~235 K on heating. Furthermore, presence of hysteresis in the inverse magnetic susceptibility during cooling and heating is indicative of a first-order nature of the transformation. The physical properties agree well with crystallographic data described in the previous section. As also indicated in Fig. 5,

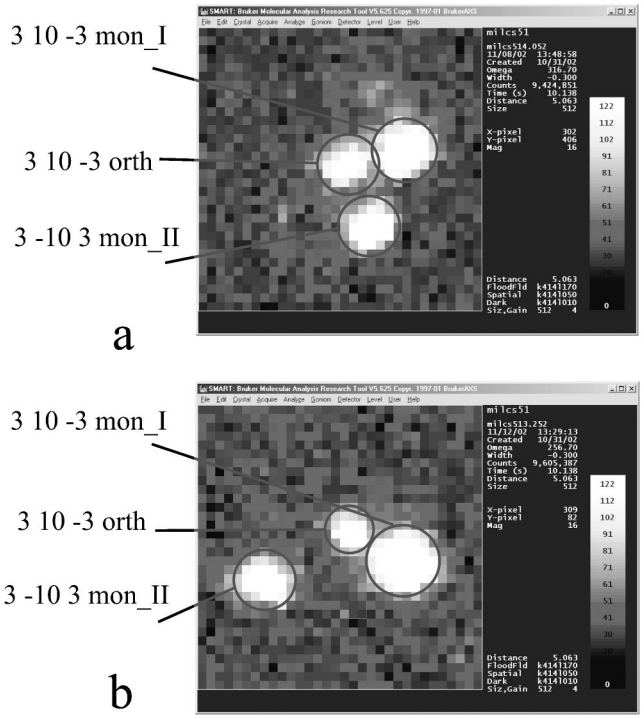

FIG. 4. Distortion of the monoclinic lattice II towards the orthorhombic lattice 9.5 h after the temperature was stabilized. (a) Reflection 3 −10 3 of the monoclinic twin component II comes close to reflection 3 10 −3 of the orthorhombic component. (b) The same reflections are more separated 2 hour earlier. The reflections in (a) and (b) are observed at $\varphi = 180°$ and 270°, respectively.

the low-temperature polymorph of erbium silicide will be referred to as the α form and the high-temperature modification is named the β form. The x-ray single crystal refinement yielded stoichiometric Er_5Si_4 within the experimental errors and confirmed an orthorhombic Gd_5Si_4-type structure for the β form. The α modification has a monoclinic $Gd_5Si_2Ge_2$ structure.[2,4] The temperature-induced structural change in Er_5Si_4 can be also monitored through lattice parameters (Fig. 6). Discontinuous variations of the unit cell dimensions at 222 K, as well as sudden formation (or disappearance) of Bragg reflections corresponding to different lattices, support the notion that the transition is a first-order one. A large change in the *a* parameter (0.81%) is consistent with the data from related systems undergoing similar orthorhombic-monoclinic (*O*-*M*) distortions, e.g., $Gd_5Si_{4-x}Ge_x$ alloys with $x \approx 2$.[18] A few degrees below and at the transition point, all lattice dimensions exhibit significant nonlinear increases before relaxing to their respective final values. Furthermore, the lattice parameters of both the orthorhombic and monoclinic phases in the vicinity of the phase transformation temperature (222 K) are always smaller than those more than 5 K away from the transition temperature. Choe *et al.*[33] observed a similar decrease in the *a* parameter below the transition temperature for a $Gd_5Si_{1.5}Ge_{2.5}$ single crystal. Although the natures of these anomalies are at present unknown, presence of intermediate states might be an explanation. Existence of some intermediate states for both the orthorhombic and monoclinic lattices is rather obvious at the

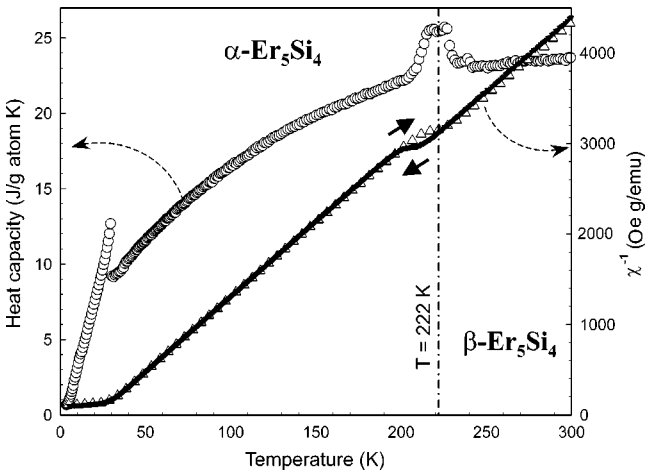

FIG. 5. Heat capacity of Er_5Si_4 measured on heating in zero magnetic field (open circles, left-hand scale) and inverse magnetic susceptibility measured in a 10 kOe magnetic field on both heating (open triangles) and cooling (closed triangles, right-hand scale). The arrows indicate the direction of temperature change. The vertical dash-dotted line indicates the temperature at which the phase transition process has been monitored using single crystal diffraction experiment.

transition point if one recalls a gradual development of the orthorhombic and distortion of the monoclinic II lattices, which occur over an extended period of time at 222 K.

The *O*-*M* transition in Er_5Si_4 is fully reversible as shown by cycling through the transition temperature. Similar to the $Gd_5Si_2Ge_2$ phase, this transformation is remarkable in a sense that it involves breaking and forming covalentlike

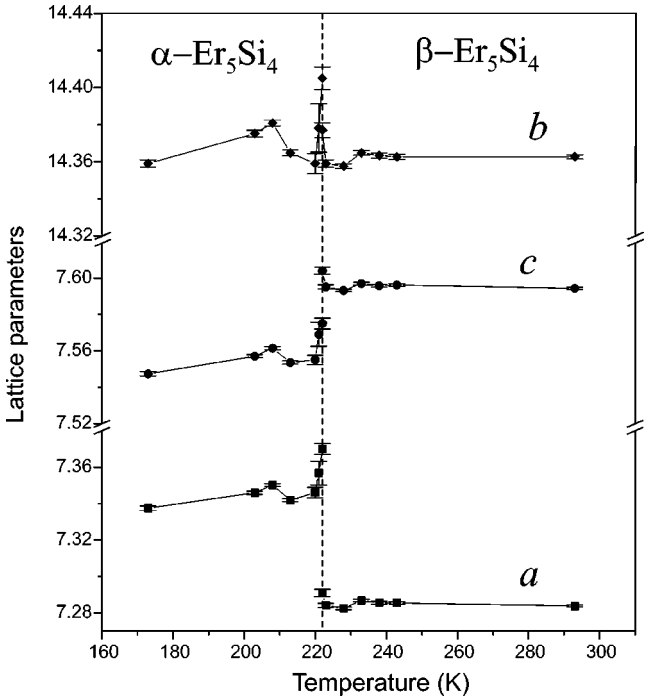

FIG. 6. Lattice parameters as functions of temperature determined during heating from 173 to 293 K. The dashed line indicates the transition temperature of 222 K.

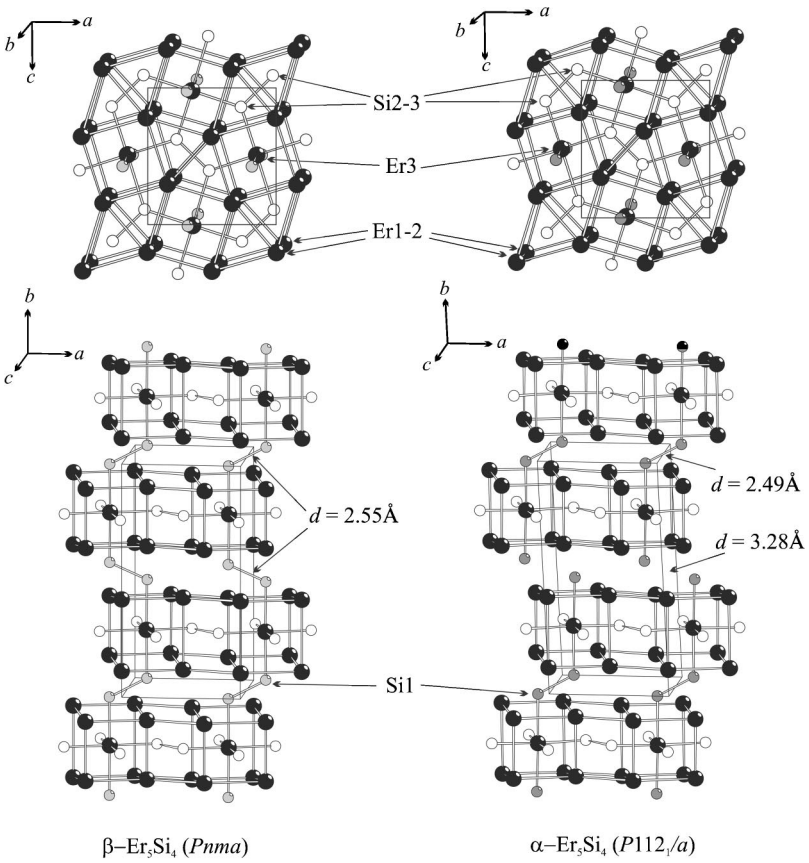

FIG. 7. Crystal structures of orthorhombic β-Er_5Si_4 and monoclinic α-Er_5Si_4, projected along the *b* and *c* axes. The top projections emphasize the Er (3^2434) nets with the Er3 in pseudotetragonal and Si2-3 in trigonal prismatic voids. In α-Er_5Si_4 half of the Si1-Si1 dimers between the slabs are broken.

bonds between Si atoms. Such solid state, first-order phase transitions typically occur with changes in much weaker interactions, such as hydrogen bonding[34,35] or van der Waals forces,[36] because changes in covalent bonding often result in the irreversible formation of a new phase.[37] Reversible *O-M* distortions were also observed in other related systems [e.g., $R_5Si_{4-x}Ge_x$, R=Gd, Tb, Dy (Refs. 38, 39, 19)], yet several features distinguish the transition in Er_5Si_4 from those for the other members of this family of materials. First, the observed sequence of structures in Er_5Si_4 is unusual in that the erbium silicide is the only known phase, where the reversible *O-M* transition occurs upon cooling below the room temperature, and is not coupled with the magnetic ordering. Second, previous examples of the *O-M* transition were observed in the systems containing both Si and Ge, i.e., in those where there is an additional degree of structural freedom provided by the potential variability of Si and Ge occupancies of the respective sites. Third, although Er_5Si_4 is twinned, as are $Gd_5Si_2Ge_2$ (Ref. 18) and $Gd_5Si_{1.5}Ge_{2.5}$,[33] the *O-M* twin law in Er_5Si_4 appears to be different.

Atomic model for twinning in monoclinic Er_5Si_4

The orthorhombic Er_5Si_4 structure is built from nearly identical 3^2434 nets (in Schläffli notation) of Er atoms (Fig. 7). Two such nets are placed over one another along the *b* axis to form two-dimensional slabs with Er3 in pseudotetragonal and Si2-3 in trigonal prismatic voids. Whereas in β-Er_5Si_4 each slab is linked through Si1-Si1 dimers with two neighboring slabs, in α-Er_5Si_4 each slab is bonded only to one neighboring slab. Thus, the monoclinic structure can be obtained from the orthorhombic structure, when alternating layers of Si1-Si1 dimers are broken as adjacent pairs of slabs shift in opposite directions along the *a* axis as illustrated in Fig. 8(a) ($d_{\text{Si-Si}}$=2.55 Å in the orthorhombic structure increases to 3.28 Å between the slabs where the Si1-Si1 bonds have been broken, while the distance slightly shortens to 2.49 Å where the dimers are still intact). This pathway yields an untwinned crystal. On the other hand, if two adjacent layers of Si1-Si1 dimers are broken, then two equivalent monoclinic cells with different orientations are generated [Fig. 8(b)]. The two monoclinic lattices share the *ac* plane and are related by a 180° rotation around the *a* axis. One interesting feature of this model is that a single false shear movement of the slabs will generate a macroscopic monoclinic twin. If there are many such irregular movements, microscopic twins are obtained. Single-crystal x-ray diffraction provides experimental data integrated over the volume of the entire specimen, and, therefore, offers no way of distinguishing whether twinning is macroscopic or microscopic in Er_5Si_4. We can assume, however, that if one fault can develop, the chances are that more random faults will occur. In addition, selective area diffraction experiments on monoclinic $Gd_5Si_2Ge_2$, which has a similar structure and twinning, indicated microscopic twinning.[26]

Coexistence of the orthorhombic and monoclinic phases

Presence of several crystalline domains of the same phase in a single crystal, as in monoclinic Er_5Si_4, is a rather com-

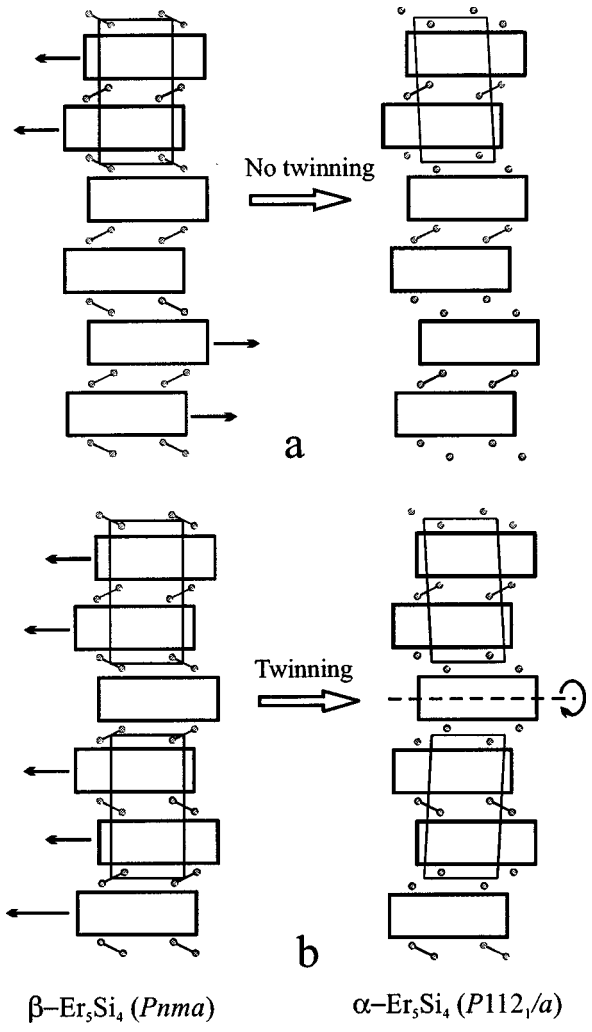

FIG. 8. (a) Untwinned pathway for the orthorhombic-to-monoclinic transformation in Er_5Si_4 through the shear movement of the slabs along the *a* axis. (b) Twinned pathway for the same transition. The figures on the left represent the orthorhombic structure and the ones on the right show the untwinned or twinned monoclinic structures. The dashed line indicates the twin axis.

mon phenomenon.[40,41] More rare is the coexistence of two phases across the transition point in a single crystal. First, this is only possible in a first-order transition and, second, fixing this state in terms of intensive variables (temperature, pressure, etc.) is challenging for a small single crystal. Choe *et al.*[33] observed the presence of an orthorhombic Sm_5Ge_4-type and two twinned monoclinic $Gd_5Si_2Ge_2$-type components in crystals of $Gd_5Si_{1.5}Ge_{2.5}$ at room temperature. The coexistence of the two phases, which have different Si/Ge ratios and are separated by a two-phase region, results from an inhomogeneous composition in crystals. All three components in $Gd_5Si_{1.5}Ge_{2.5}$ share the *a* axis, which is also a rotation twin axis for the monoclinic components. In the case of Er_5Si_4, composition is not a variable, thus temperature, which can be controlled in our experiment, rendered a state in which the two phases coexist. This state is qualitatively different from one in $Gd_5Si_{1.5}Ge_{2.5}$, since it is an equilibrium state. Small temperature variations (± 1 K in our experiments) were sufficient to shift the equilibrium and trigger the formation/disappearance of the orthorhombic/monoclinic lattices, respectively.

Based on the orientations of the monoclinic and orthorhombic lattices in the Er_5Si_4 crystal [see Fig. 3(b)], we can model the interface between the α and β forms. Conceptually, the transition between the two structures during heating is the reverse to the one in Fig. 8(a), but the actual pathway is somewhat different. The two double slabs of the monoclinic structure do not just slide along the *a* axis, they also rotate slightly around the *c* axis [Fig. 9(a)]. As can be seen in Fig. 9(b), it is possible to stack the Gd_5Si_4-type fragments over the $Gd_5Si_2Ge_2$-type ones. However, due to the tilt between the slabs of the two types, the fused *ac* plane cannot be infinite; at some point it has to jump to the next slab in order to propagate in the same direction. A stacking fault must form and the two phases must be separated by a domain boundary along the *b* direction. This is different from the orthorhombic-monoclinic coexistence in $Gd_5Si_{1.5}Ge_{2.5}$, in which the orthorhombic Sm_5Ge_5-type and monoclinic $Gd_5Si_2Ge_2$-type structures share the *ac* plane.[33]

Landau theory, normal modes, and structural transition in Er_5Si_4

To understand the *O*-*M* transition on the atomic scale we performed a symmetry analysis of the vibrational modes in Er_5Si_4. A normal mode responsible for the observed symmetry lowering can be identified from the space groups of the low- and high-symmetry structures. Such analysis is possible because the two space groups $Pnma$ and $P112_1/a$ are in a group-subgroup relationship. Using Landau theory,[29,42] it is possible to show that the B_{1g} mode would produce the $P112_1/a$ cell of the correct basis from the $Pnma$ space group (B_{1g} is a notation for the irreducible representation in the D_{2h} point group and it determines the symmetry of the normal mode). If this B_{1g} mode is involved in the distortion, there must be atoms in the orthorhombic structure whose vibrations are of that symmetry and, besides, there must be noticeable atomic shifts caused by this normal mode.

Since the distortion from the orthorhombic structure to the monoclinic structure in Er_5Si_4 does not result in a loss of any translations, i.e., no superstructure is formed, the wave vector $\mathbf{k}$ of the distortion is $\mathbf{k}=0$. Thus, the normal modes of interest are restricted to one unit cell and they can be described in terms of the irreducible representations of the point group D_{2h} of the space group $Pnma$. There are 108 characteristic modes ($N=36$ atoms in the primitive unit cell), of which three are the translational degrees of freedom (these are B_{1u}, B_{2u}, B_{3u}). The 108 vibrational modes were determined using group theoretical techniques and all modes are assigned to the six inequivalent sites as follows:

$$\text{Er1, Er2, Si1: } 3A_g+3B_{1g}+3B_{2g}+3B_{3g}+3A_u+3B_{1u}+3B_{2u}+3B_{3u},$$

$$\text{Er3, Si2, Si3: } 2A_g+B_{1g}+2B_{2g}+B_{3g}+A_u+2B_{1u}+B_{2u}+2B_{3u}.$$

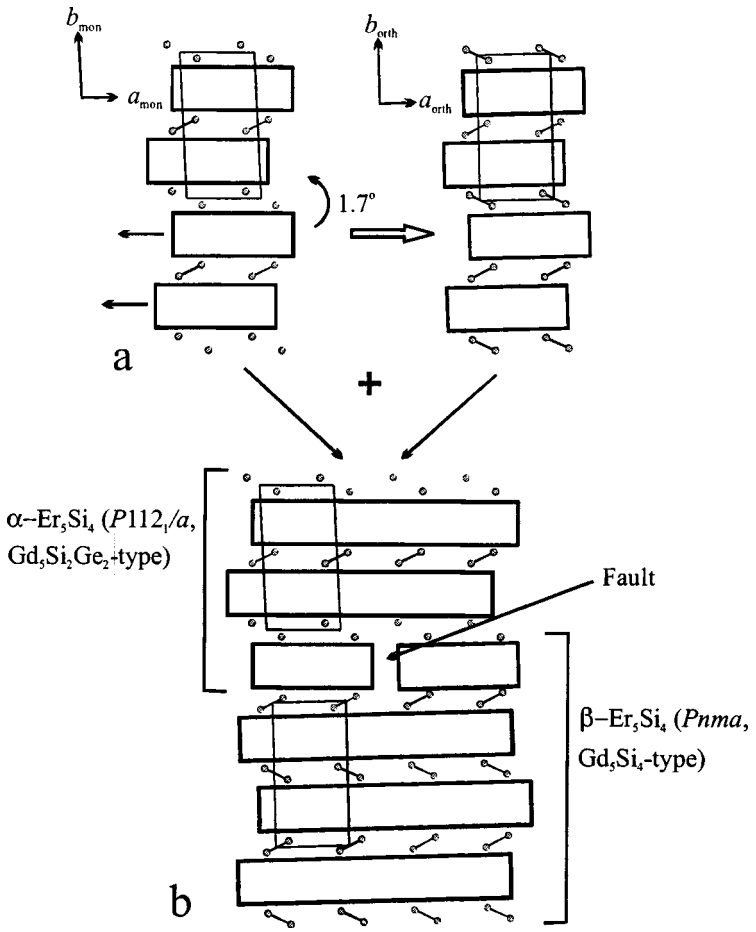

FIG. 9. (a) Transformation of the monoclinic $Gd_5Si_2Ge_2$-type structure into the orthorhombic Gd_5Si_4-type structure through the shear movement and rotation of the slabs in the single crystal of Er_5Si_4. (b) Interface between the two structures. Formation of the fault is necessary in order for the fusion ac plane to propagate.

The B_{1g} mode, that reduces the symmetry from $Pnma$ to $P112_1/a$, is present in the vibrations of all the atoms. Rotational shifts around the z axis belong to the B_{1g} irreducible representation. Three such shifts for the Si1, Si2, and Si3 atoms are shown in Fig. 10(a). These B_{1g} shifts are antisymmetric (atoms move in the opposite directions) with respect to the mirror plane at $y=\frac{1}{2}$ that separates the two slabs, shear movements of which break half of the Si1-Si1 bonds. The B_{1g} normal modes will produce a monoclinic structure in which the slabs and the a axis, collinear with the slabs, are rotated around the c axis with respect to those in the orthorhombic structure. An experimental proof of the correspondence of the O-M transition to the B_{1g} irreducible representation comes from the mutual orientation of the orthorhombic and monoclinic lattices at the transition point [Fig. 3(b)].

B_{1g}-type shifts of *any* of the atoms would be sufficient to cause the symmetry reduction. The rearrangement of the whole structure, as seen during the O-M transition in Er_5Si_4, however, is possible only when *all* the atoms undergo the B_{1g} shifts. Thus, this structural distortion corresponds to six independent B_{1g} irreducible representations and not one, as required by Landau theory for a second-order transition, and, therefore it must, be a first-order transition. On the atomic scale, the second-order nature would have required all atoms to move simultaneously and continuously to achieve the atomic positions and spatial orientation of the monoclinic structure, which is an unlikely event. It is more probable that at some time the superposition of the B_{1g} vibrational modes of the six independent atoms will lead to a sudden change in the atomic arrangement.

To understand the shear movement of the slabs, we can decompose the B_{1g} rotational shifts into a number of small

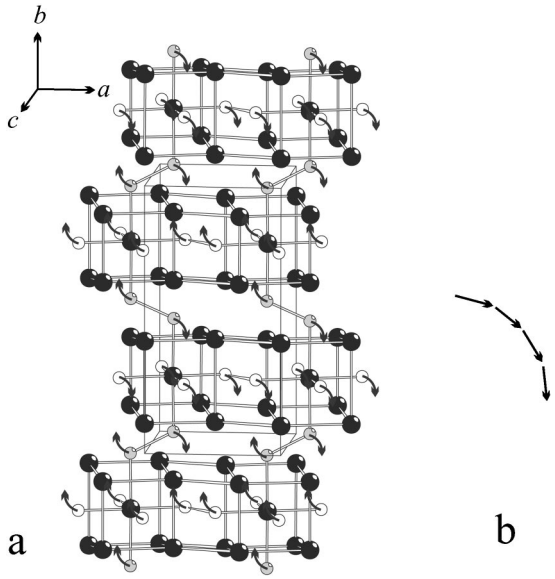

FIG. 10. (a) B_{1g} rotational shifts of Si1, Si2, and Si3 atoms in β-Er_5Si_4 ($Pnma$). (b) Decomposition of the B_{1g} rotational shift into a number of vectors in the ab plane.

TABLE III. Parameters for the extended Hückel tight-binding calculations.

Atom	Orbital	H_{ii}, eV	ξ_1	c_1[a]	ξ_2	c_2[a]
Er	6s	−8.45	1.54	1.00		
Er	6p	−5.54	1.54	1.00		
Er	5d	−7.94	2.810	0.7063	1.2160	0.4834
Si	3s	−17.30	1.383	1.00		
Si	3p	−9.20	1.383	1.00		

[a]Coefficients used in the double-zeta Slater-type orbitals.

vectors in the ab plane [Fig. 10(b)]. The first vector has the largest contribution along the a axis, whereas the last one has the largest contribution along the b axis. The shifts along these two vectors will try to ''shear'' move the slabs along the a direction and to separate or bring them closer in an alternating fashion along the b direction. If the former process is a possible event, the latter one is an unlikely scenario in the structure of Er_5Si_4. This argument is consistent with a large change in the a parameter (0.81%) and a small one in the b parameter (−0.07%).

Calculated electronic structures of orthorhombic and monoclinic Er_5Si_4

To gain further insights into driving forces of the O-M distortion, tight-binding linear-muffin-tin-orbital calculations with the atomic sphere approximation (TB-LMTO-ASA)[43] were carried out using the crystallographic data of the low- and high-temperature forms of Er_5Si_4. To satisfy the overlap criteria of the atomic spheres in the LMTO-ASA method, empty spheres were included in the unit cell (76 in the orthorhombic and 48 in the monoclinic cell, employing automatic sphere generation). (Calculations without empty spheres produced a wrong relative position of the Fermi level for the monoclinic structure. These calculations are not considered here.) The $4f$ electrons of Er were treated as core electrons, which is a good approximation due to the fact that both structures are paramagnetic. Since presence and number of the empty spheres influences the overlap between the atoms, Mulliken overlap populations within the Hückel tight-binding method (EHTB)[44] were calculated to analyze interactions between specific atoms in the two structures. The energies for Er and Si orbitals (Table III) were taken from Ref. 45, the Er energies were then refined through charge iteration. Both TB-LMTO-ASA and EHTB methods produced similar densities of states (DOS) and crystal orbital Hamilton/overlap population (COHP/COOP) curves for the two structures. Only DOS and COHP plots, obtained from the TB-LMTO-ASA calculations, are presented here.

Room-temperature orthorhombic β-Er_5Si_4

In the room-temperature orthorhombic structure of β-Er_5Si_4, all Si atoms form either interslab Si1-Si1 dimers of 2.55 Å or intraslab Si2-Si3 dimers of 2.53 Å. According to the Zintl-Klemm electron counting formalism for valence compounds,[46] the Si_2 dimers are isoelectronic with halogen dimers and carry a formal negative charge of −6. If Er atoms are considered as Er^{3+}, the chemical formula of the orthorhombic phase can be written as $(Er^{3+})_5(Si_2^{6-})_2(3e^-)$. Three remaining valence electrons will occupy Er-Er bonding states, and also Si-Si $3p$ antibonding states. Because the Er-Er bonding states are dispersed in energy due to rather strong interactions (as judged from corresponding distances), and the number of electrons is obviously not sufficient to occupy all bonding states, the Fermi level is expected to lie in the middle of the conduction band and Er_5Si_4 is expected to be a metal.

This simple reasoning is supported by calculated DOS's and COHP's (Figs. 11, 12). Two peaks around −9.5 and −7 eV represent the bonding σ_s and antibonding σ_s^* states of the Si_2 dimers, with contribution from the Er orbitals. The valence band, which extends from −5 up to −1 eV, is separated by a small energy gap of 0.2 eV from the conduction band. The states below −1 eV are derived from $3p$ lone pairs of Si_2 dimers, which interact in a bonding manner with Er $6s$ and $5d$ orbitals, that are also involved in the Er-Er bonding. The conduction band, above −1 eV, has the largest contribution from Er $5d$ and $6p$ orbitals and small contribution from the σ_p^* states within the Si_2 dimers. Analysis of the bond characters [see COHP curves in Figs. 12(a), 12(b)] indicates bonding Er-Er and Er-Si interactions, antibonding interslab and intraslab Si-Si interactions around the Fermi level. Therefore, reducing the number of itinerant electrons will favor Si-Si bonding but will weaken the other interactions. The solution to this dilemma comes as a shear movement of the slabs, which breaks half of the interslab Si-Si bonds and creates a monoclinic structure at low temperatures.

Low-temperature monoclinic α-Er_5Si_4

Breaking half of the interslab Si1-Si1 bonds gives 1.5 Si_2 dimers and one Si1 monomer per formula unit. Treating the Si1B monomers to be isoelectronic with noble gas atoms and to carry formal negative charge of −4, we can write the chemical formula of monoclinic α-Er_5Si_4 as $(Er^{3+})_5(Si_2^{6-})_{1.5}(Si^{4-})(2e^-)$, which indicates one less electron in the conduction band and results in a lower energy of the Fermi level ($E_F = -0.48$ eV vs −0.39 eV). Presence of the chemically different Si^{4-} monomers with very weak interactions to other Si^{4-} affects the DOS. The two most prominent features in the DOS of monoclinic Er_5Si_4 are (i) appearance of an additional DOS peak just below −8 eV and (ii) a smaller band gap below −1 eV ($\Delta E = 0.05$ eV vs 0.20 eV). The changes in the DOS are direct consequences of dimer breaking. Since the Si1B-Si1B interaction are weak ($d_{\text{Si1B-Si1B}} = 3.28$ Å at 203 K), the separation between the bonding σ_s and antibonding σ_s^* Si1B states is small. While the antibonding states overlap with the antibonding state of other Si atoms, the bonding states fall in the energy gap. Small energetic dispersion is also observed for the bonding σ_p and antibonding σ_p^* Si1B states, which builds up electronic states around −1 eV and, thus, narrows the band gap. The DOS changes in Er_5Si_4 are consistent with those observed for the O-M transition in $Gd_5Si_2Ge_2$.[21]

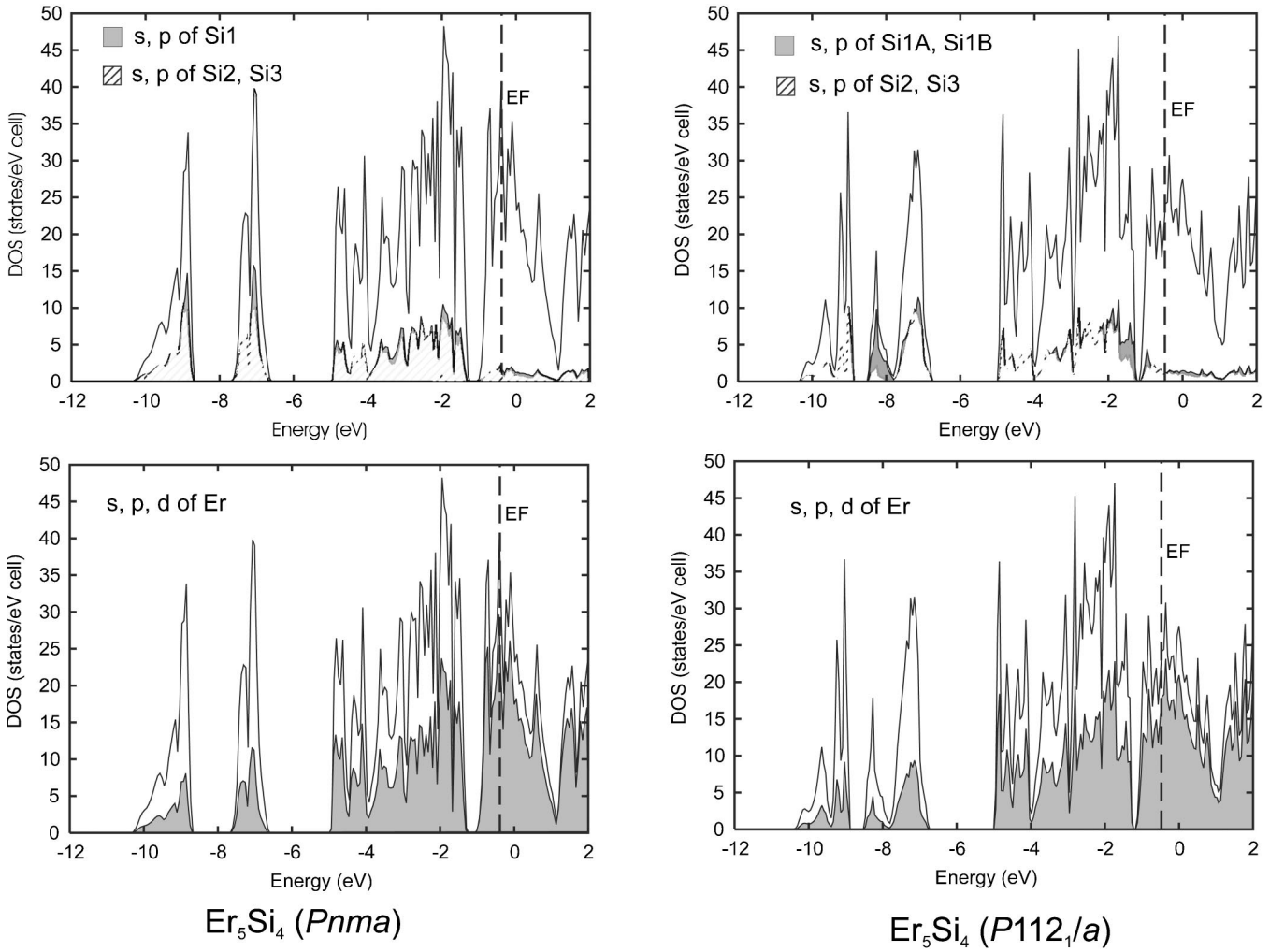

FIG. 11. Total and projected densities of states (DOS) for orthorhombic and monoclinic Er_5Si_4.

Bonding in orthorhombic and monoclinic Er_5Si_4

Since the low-temperature monoclinic structure of Er_5Si_4 is a low symmetry structure, it must be energetically stabilized upon distortion. While reducing the number of conduction electrons would strengthen Si-Si bonding, a complete bond cleavage, as found in monoclinic Er_5Si_4, would not favor the overall Si-Si bonding. Therefore, a detailed analysis of interactions was performed to gain some insights into the phase stability and energetic aspects of the transition. To evaluate bonding, two parameters were used: bond distance and Mulliken overlap population (MOP) as a measure of bond strength (only bonds with $d \leqslant 4.2$ Å are considered). Although highly correlated with bond distance, bond strength can be small for a short interatomic distance and large for a long one. This phenomenon is known as a ''matrix effect:'' a separation, fixed by the geometric factors, is more important than the nearest neighbor interaction. Matrix effects are observed for some bonds within each structure, but there is, in general, a good distance/strength correlation between similar bonds of the two structures.

The structural considerations, as well as calculated MOP's, indicate nearly negligible perturbations within the slabs, e.g., the average Er-Er distances in the ac plane, average Er-Si2, Er-Si3 bonds within the slabs and corresponding MOPs have similar values for the two structures (Table IV). Also the majority of the interactions (Er-Er and Er-Si1) between the slabs with Si1-Si1 dimers intact are analogous in both orthorhombic and monoclinic Er_5Si_4 (Table IV). There is a substantial strengthening of Si1-Si1 dimers, but since there are only two such dimers per unit cell in monoclinic α-Er_5Si_4, it is safe to consider such interslab bonds to be similar, on average, between the two structures. On the other hand, there are significant changes in bonding between the slabs that move with respect to each other (Fig. 13). The interslab bonds of interest are divided into three groups Si1-Si1, Er-Er, and Er-Si1 (Si1B-Si1B and Er-Si1B in the monoclinic structure). Furthermore, the Er-Si1 bonds are separated into the bonds that Si1 form to its ''own'' slab, which are white in Fig. 13, and the bonds that Si1 makes to the ''opposite'' slab, shown as dark lines. Although artificial, this division of the Er-Si1 bonds has a structural sense: while the surrounding of Si1 with respect to its ''own'' slab remains nearly the same upon distortion, there is a significant change in its surrounding with respect to the ''opposite'' slab upon the transition.

As indicated before, the Si1-Si1 interactions within the broken dimers (Si1B-Si1B in monoclinic structure) are much

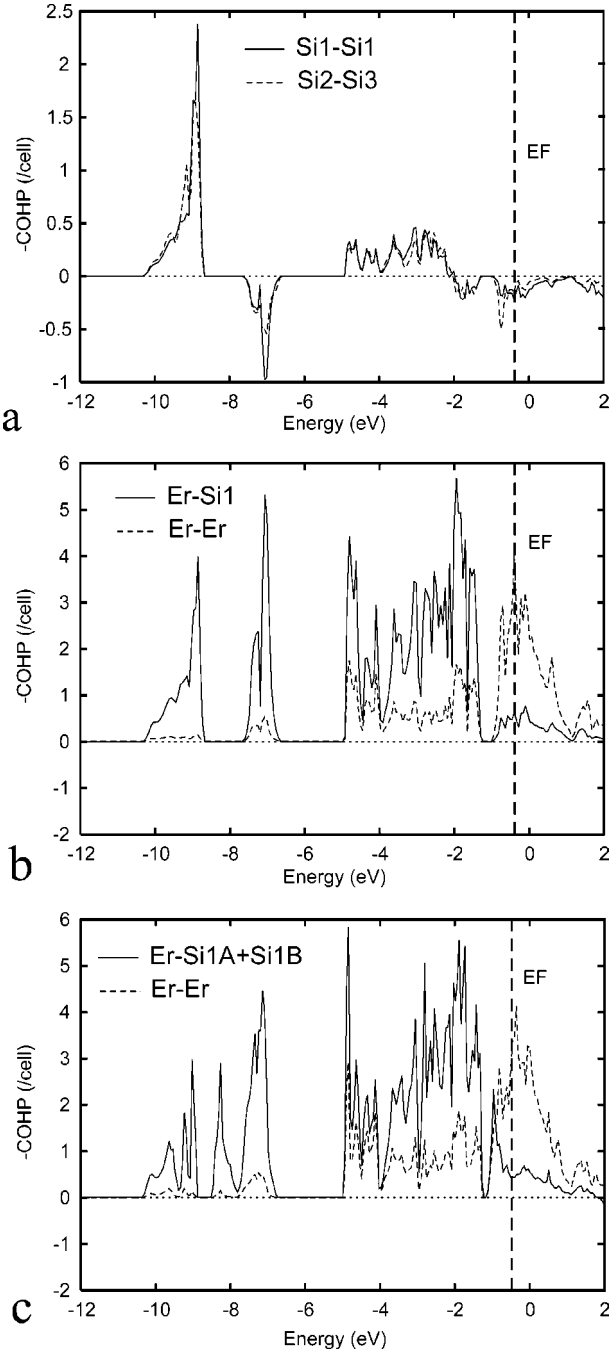

FIG. 12. Crystal orbital overlap population (COHP) curves for some interactions in orthorhombic [(a), (b)] and monoclinic (c) Er_5Si_4. Interactions in the upper part are bonding, in the lower part antibonding.

weaker in α-Er_5Si_4 (Table IV). Out of the three interslab Er-Er bonds of 3.62, 3.85, and 3.90 Å (MOP=0.172, 0.159, and 0.179) in β-Er_5Si_4, only the first one becomes stronger in the monoclinic phase (d=3.46 Å, MOP=0.196), whereas the other bonds become weaker (d=4.20, 3.91 Å and MOP=0.057, 0.134). As a result, the overall interslab Er-Er interactions are weaker in the monoclinic structure. With the exception of one bond of 3.10/3.34 Å, the Er-Si1 bonds, either to its ''own'' side or to the ''opposite'' side

TABLE IV. Comparison of average interatomic distances and Mulliken overlap populations (MOP's) for the orthorhombic and monoclinic structures of Er_5Si_4. Number of bonds per unit cell is given in parentheses.

	β-Er_5Si_4 ($Pnma$)		α-Er_5Si_4 ($P112_1/a$)	
Bonds	d, Å	MOP	d, Å	MOP
Er-Er interactions in the ac plane within the slabs				
Er-Er (×40)	3.856	0.133	3.859	0.126
Er-Si2, Er-Si3 and Si2-Si3 interactions whithin the slabs				
Er-Si2 (×32)	2.974	0.343	2.977	0.344
Er-Si3 (×32)	3.003	0.342	3.000	0.343
Si2-Si3 (×4)	2.534	0.498	2.559	0.479
Er-Er, Er-Si1 and Si1-Si1 interactions between the slabs connected via Si1-Si1 dimers[a]				
Er-Er (×10)	3.768	0.168	3.790	0.164
Er-Si1 (×32)	3.027	0.337	3.045	0.331
Si1-Si1 (×2)	2.549	0.501	2.488	0.551
Er-Er, Er-Si1 and Si1-Si1 interactions between the slabs not connected via Si1-Si1 dimers[a]				
Er-Er (×10)	3.768	0.168	3.845	0.128
Er-Si1 (×20)[b]	2.961	0.364	2.940	0.404
Er-Si1 (×12)[c]	3.136	0.291	3.085	0.351
Si1-Si1 (×2)	2.549	0.501	3.279	0.066

[a]Number of Er-Er, Er-Si1, and Si1-Si1 interactions is doubled in the orthorhombic structure.
[b]Er-Si1 interactions to its ''own'' side (see text for explanations).
[c]Er-Si1 interactions to the ''opposite'' side.

become stronger upon symmetry breaking, despite the fact that some bonds are longer in monoclinic α-Er_5Si_4. The largest increase is observed for the interaction between the Si1 atoms (Si1B in monoclinic Er_5Si_4) and the Er atoms of the ''opposite'' side (Table IV). The strengthening of the Er-Si1 interactions in the monoclinic structure is intuitively expected from chemical considerations, since the Si1 electrons, freed from bonding in the Si_2 dimers, are donated to the Er-Si1 interactions. The COHP calculations by the LMTO method also support this argument. Appearance of the two peaks in the Er-Si1 bonding region around the band gap at -1 eV is a direct consequence of the dimer breaking. There is an additional electron transfer from the weaker interslab Er-Er bonds to the Er-Si1 bonds, as well as to the Er-Si2 and Er-Si3 bonds inside the slabs. That is why there is a small increase in the MOPs for the Er-Si2 and Er-Si3 interactions, although the Fermi level falls lower upon transition.

Thus, the O-M transition is an energetic trade off in interactions. In general, the Er-Si bonds, specially the Er-Si1 ones, become stronger, whereas the Er-Er and Si-Si bonds become weaker in α-Er_5Si_4. EHTB calculations predict lower total electronic energy by 1.99 eV/cell for the monoclinic structure. Although more exact calculations of the total energies need to be performed, it is safe to say that the monoclinic phase is electronically more favorable, and that this electronic stabilization is achieved through the O-M structural rearrangement.

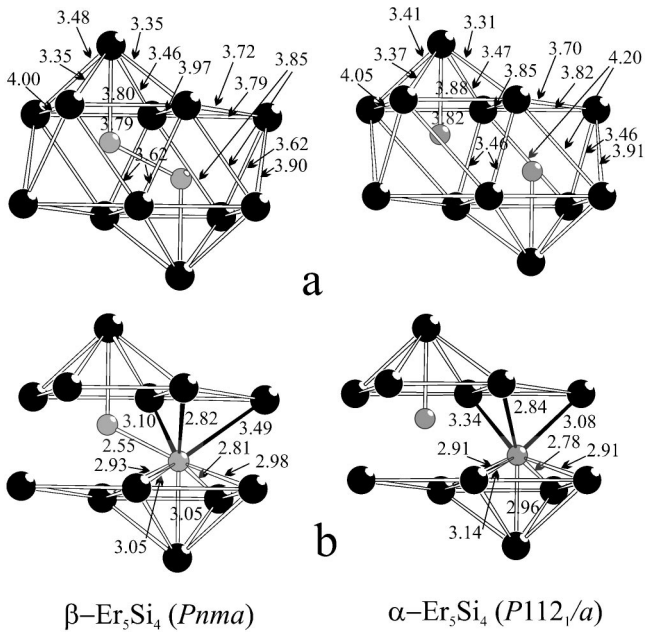

FIG. 13. (a) Er-Er interslab and some intraslab distances in orthorhombic β- and monoclinic α-Er_5Si_4. (b) Er-Si1 distances between the slabs. Bonds to its ''own'' layer are white and bonds to the ''opposite'' layer are black. Er atoms are black, Si atoms are gray.

While the symmetry breaking in Er_5Si_4 is energetically driven, the reverse transition to the orthorhombic structure at high temperatures is entropically governed ($\Delta S > 0$). This is due to the fact that a high-symmetry structure has a higher entropy (higher degeneracy of the electronic and vibrational states) and, thus, it is preferred at high temperatures. This stability argument can be extended to other R_5X_4 phases. Obviously, each specific case will have its own particularities, e.g., strength of R-X interactions in R_5X_4 or appearance of ferromagnetism and associated changes in the band structure, as in some of the Gd_5X_4 phases.

CONCLUSIONS

Er_5Si_4 exhibits a reversible, temperature-induced transformation between the high-temperature orthorhombic and low-temperature monoclinic polymorphs. Although the structural sequence is opposite to those observed in other R_5X_4 materials below room temperature, the distortion follows the conventional Gibbs free energy/entropy relationship due to decoupling of the structural and magnetic transitions. While optimization of Er-Si interactions upon the O-M transition minimizes the electronic energy for the low-temperature monoclinic form, increased entropy stabilizes the orthorhombic form at high temperatures. On the atomic scale, the distortion corresponds to the B_{1g} normal mode that induces shear movement along the a axis and rotation of slabs around the c axis. One of structural consequences of the B_{1g} mode is that the monoclinic and orthorhombic lattices share only the c axis during the transition. The O-M transformation leads to intrinsic twinning, possibly microscopic, in the monoclinic phase.

ACKNOWLEDGMENTS

This manuscript has been authored by Iowa State University of Science and Technology under Contract No. W-7405-ENG-82 with the U.S. Department of Energy. The research was supported by the Office of the Basic Energy Sciences, Materials Sciences Division, U.S. DOE.

*Email address: gmiller@iastate.edu

[1] F. Holtzberg, R. J. Gambino, and T. R. McGuire, J. Phys. Chem. Solids **28**, 2283 (1967).
[2] V. K. Pecharsky and K. A. Gschneidner, Jr., Phys. Rev. Lett. **78**, 4494 (1997).
[3] V. K. Pecharsky and K. A. Gschneidner, Jr., J. Magn. Magn. Mater. **167**, L179 (1997).
[4] V. K. Pecharsky and K. A. Gschneidner, Jr., J. Alloys Compd. **260**, 98 (1997).
[5] V. K. Pecharsky and K. A. Gschneidner, Jr., J. Magn. Magn. Mater. **200**, 44 (1999).
[6] K. A. Gschneidner, Jr. and V. K. Pecharsky, Annu. Rev. Mater. Sci. **30**, 387 (2000).
[7] L. Morellon, P. A. Algarabel, M. R. Ibarra, J. Blasco, B. García-Landa, Z. Arnold, and F. Albertini, Phys. Rev. B **58**, R14 721 (1998).
[8] L. Morellon, J. Stankiewicz, B. García-Landa, P. A. Algarabel, and M. R. Ibarra, Appl. Phys. Lett. **73**, 3462 (1998).
[9] E. M. Levin, V. K. Pecharsky, and K. A. Gschneidner, Jr., Phys. Rev. B **60**, 7993 (1999).
[10] C. Ritter, L. Morellon, P. A. Algarabel, C. Magen, and M. R. Ibarra, Phys. Rev. B **65**, 094405 (2002).
[11] H. B. Wang, Z. Altounian, and D. H. Ryan, Phys. Rev. B **66**, 214413 (2002).
[12] O. Tegus, O. Dagula, E. Brück, L. Zhang, F. R. de Boer, and K. H. J. Buschow, J. Appl. Phys. **91**, 8534 (2002).
[13] H. F. Yang, G. H. Rao, G. Y. Liu, Z. W. Ouyang, X. M. Feng, W. F. Liu, W. G. Chu, and J. K. Liang, J. Phys.: Condens. Matter **14**, 9705 (2002).
[14] C. Magen, Z. Arnold, L. Morellon, Y. Skorokhod, P. A. Algarabel, M. R. Ibarra, and J. Kamarad, Phys. Rev. Lett. **91**, 207202 (2003).
[15] D. H. Ryan, M. Elouneg-Jamróz, J. van Lierop, Z. Altounian, and H. B. Wang, Phys. Rev. Lett. **90**, 117202 (2003).
[16] V. K. Pecharsky, A. P. Holm, K. A. Gschneidner, Jr., and R. Rink, Phys. Rev. Lett. **91**, 197204 (2003).
[17] V. K. Pecharsky and K. A. Gschneidner, Jr., Adv. Mater. (Weinheim, Ger.) **13**, 683 (2001).
[18] W. Choe, V. K. Pecharsky, A. O. Pecharsky, K. A. Gschneidner, Jr., V. G. Young, Jr., and G. J. Miller, Phys. Rev. Lett. **84**, 4617 (2000).
[19] A. O. Pecharsky, K. A. Gschneidner, Jr., V. K. Pecharsky, and C. E. Schindler, J. Alloys Compd. **338**, 126 (2002).
[20] H. F. Franzen, *Physical Chemistry of Inorganic Crystalline Solids* (Springer-Verlag, New York, 1986).
[21] V. K. Pecharsky, G. D. Samolyuk, V. P. Antropov, A. O. Pecharsky, and K. A. Gschneidner, Jr., J. Solid State Chem. **171**, 57 (2003).

[22] V. K. Pecharsky, A. O. Pecharsky, and K. A. Gschneidner, Jr., J. Alloys Compd. **344**, 362 (2002).
[23] V. K. Pecharsky, A. O. Pecharsky, Y. Mozharivskyj, K. A. Gschneidner, Jr., and G. J. Miller, Phys. Rev. Lett. **91**, 207205 (2003).
[24] XRD Single Crystal Software (Bruker Analytical X-Ray Systems, Madison, USA, 2002).
[25] *Binary Alloy Phase Diagrams*, edited by T. B. Massalski, H. Okamoto, P. R. Subramanian, and L. Kacprzak (ASM International, Materials Park, OH, 1990).
[26] J. Meyers, S. Chumbley, W. Choe, and G. J. Miller, Phys. Rev. B **66**, 012106 (2002).
[27] R. Herbst-Irmer and G. M. Sheldrick, Acta Crystallogr., Sect. B: Struct. Sci. **54**, 443 (1998).
[28] U. Shmueli, Acta Crystallogr., Sect. A: Found. Crystallogr. **52**, 500 (1996).
[29] H. F. Franzen, *Physical Chemistry of Solids* (World Scientific, Singapore, 1994).
[30] D. L. Reger, C. A. Little, V. G. Young, Jr., and M. Pink, Inorg. Chem. **40**, 2870 (2001).
[31] D. G. Colombo, V. G. Young, Jr., and W. L. Gladfelter, Inorg. Chem. **39**, 4621 (2000).
[32] R. I. Cooper, R. O. Gould, S. Parsons, and D. J. Watkin, J. Appl. Crystallogr. **35**, 168 (2002).
[33] W. Choe, G. J. Miller, S. Chumbley, and A. O. Pecharsky, Chem. Mater. **15**, 1413 (2003).
[34] M. T. Reetz, S. Hoeger, and K. Harms, Angew. Chem. **106**, 193 (1994).
[35] A. M. Dattelbaum and J. D. Martin, Inorg. Chem. **38**, 2369 (1999).
[36] R. Boese, T. Meibach, and A. De Meijere, J. Am. Chem. Soc. **113**, 1743 (1991).
[37] N. Sidorov, V. Mitrofanov, V. Kuznetsov, A. Gutsol, V. Kalinnikov, and S. Stefanovich, Ferroelectrics **144**, 223 (1993).
[38] V. V. Ivtchenko, V. K. Pecharsky, and K. A. Gschneidner, Jr., Adv. Cryog. Eng. **46**, 405 (2000).
[39] H. Huang, A. O. Pecharsky, V. K. Pecharsky, and K. A. Gschneidner, Jr., Adv. Cryog. Eng. **48**, 11 (2002).
[40] *Fundamentals of Crystallography*, edited by C. Giacovazzo (Oxford University Press, Oxford, 1992).
[41] L. Kienle and A. Simon, J. Solid State Chem. **167**, 214 (2002).
[42] L. D. Laundau and E. M. Lifshitz, *Statistical Physics (Course of Theoretical Physics)* (Pergamon Press LTD., London-Paris, 1968), Vol. 5.
[43] O. K. Andersen and O. Jepsen, Phys. Rev. Lett. **53**, 2571 (1984).
[44] J. Ren, W. Liang, and M.-H. Whangbo, *Crystal and Electronic Structure Analyzer (CAESAR)* (North Carolina State University, Raleigh, NC, 1998).
[45] S. Alvarez, *Table of Parameters for Extended Hückel Calculations* (Barcelona, 1987).
[46] G. J. Miller, in *Chemistry, Structure, and Bonding of Zintl Phases and Ions*, edited by S. M. Kauzlarich (VCH Publishers, New York, 1996), p. 1.